Preparation, characterization, equilibrium and kinetics studies of a molecularly imprinted polymer for selective recognition of dicamba from aqueous samples

Tooraj Beyki[a], Mohammad Javad Asadollahzadeh[a,*], Mohsen Jahanshahi[b]

[a]*Department of Chemical Engineering, Shahrood Branch, Islamic Azad University, Shahrood 43189–36199, Iran,*
Tel. +98-9155202909, +98-23-32394530; emails: m.asadalahzadeh@iau-shahrood.ac.ir,
m.asadalahzadeh@gmail.com (M.J. Asadollahzadeh), Tel. +98-9355892673; email: tooraj.beyki@gmail.com (T. Beyki)
[b]*Nanotechnology Research Institute, School of Chemical Engineering, Babol University of Technology, Babol 47148–71167, Iran,*
Tel/Fax: +98-111-3220342, email: mjahan@nit.ac.ir, mmohse@yahoo.com

ABSTRACT

The aim of current study is to investigate the use of molecularly imprinted polymers (MIPs) for recognition, determination and adsorption of dicamba from aqueous samples in batch mode. Hence, the spherical MIP nanoparticles were successfully synthesized via precipitation polymerization using dicamba as a template. The synthesized polymers were then characterized by Fourier transform infrared spectroscopy, differential scanning calorimetry, scanning electron microscopy and Brunauer–Emmett–Teller analysis. Kinetic and equilibrium isotherm studies were performed using non-linear regression analysis. Finally, the selectivity of the imprinted polymer was evaluated by comparing the binding with structural analogs. The results showed that the MIP nanospheres were obtained with the average diameter of 234 nm and the specific surface area of 165.4 m^2 g^{-1}. Sips isotherm best fitted the adsorption equilibrium data, and the kinetics followed a pseudo-first-order model. In addition, the results demonstrated that the prepared imprinted polymer exhibited specific rebinding ability to its template compared with other structural analogs.

Keywords: Molecularly imprinted polymer; Molecular recognition; Precipitation polymerization; Nanospheres; Dicamba; Water treatment

1. Introduction

During recent years, the use of various herbicides and pesticides has been increasingly growing to enhance the agricultural production and protect them from pests and herbs. Although using herbicides and pesticides has provided several benefits, however, their excessive use has contaminated various water bodies including surface water, groundwater and drinking water supply by drift, runoff, drainage and leaching [1]. Exposure to some of these compounds, even at low concentrations, could have noxious effects on aquatic flora and fauna and also on human health. Consequently, the ecotoxicological effects on human health and environment have been found [2]. Dicamba (3,6-dichloro-2-methoxybenzoic acid) is a common systemic auxin-type and a low-cost herbicide,

which is extensively used for pre- and post-emergence control of annual and perennial broadleaf weeds. Since the first approvals of dicamba in 1962 [3], it has been registered in more than 100 countries worldwide for use on rye, asparagus, barley, corn, oats, soybeans, sugarcane and wheat. It is also registered for use on golf courses, residential lawns and rights-of-way along utility lines, roadsides and railways. Dicamba is very soluble in water, stable to chemical hydrolysis and highly mobile [4]. Accordingly, dicamba has been considered as one of the most frequently detected herbicides in water bodies thus far. The US Environmental Protection Agency (USEPA) has established drinking water health advisory levels for dicamba of 200 mg L^{-1} [5].

According to the statements mentioned above, the urgency for developing a selective, simple, reliable and adapted wastewater treatment process is of crucial importance. Molecular imprinting technology provides a new

* Corresponding author.

effective approach for fabrication of new polymers including specific recognition abilities for target molecules to selective determination, separation and extraction. Hence, selective uptake using molecularly imprinted polymers (MIPs) is a confident way for determination and removal of trace pollutants in water. MIPs have achieved significant popularity within the last decades as synthetic polymers with chemically selective recognition sites for determination and separation of similar or chiral compounds, purification of mixtures, chemical and biosensing, catalysis, etc. MIPs have attracted considerable interests because of their desirable molecular recognition ability, stability in harsh chemical conditions, ease and low cost of preparation, their application to a wide range of target molecules, and reusability [6–10]. Due to similarity of the specific interactions between the target molecule and MIP to that between enzyme and substrate, antibody and antigen, hormone and receptor, MIPs have found various applications in many different fields such as the stationary phase in high-performance liquid chromatography (HPLC) [11–13], solid phase extraction [14–16], sensors and biosensors [17,18], catalysts and mimic antibodies [19–21], membrane separation [22], enantioseparation [23,24] and pharmaceutical applications [25,26].

Molecular imprinting can be prepared in two ways: namely covalent imprinting (pre-organized approach) and non-covalent imprinting (self-assembly approach). These methods differ in the mechanism of interaction between the monomer and template during pre-polymerization [27]. Generally, the procedure of non-covalent imprinting is relatively simpler than covalent imprinting. In addition, guest-binding and guest-release are fast in non-covalent imprinted polymers. Furthermore, owing to the existence of polar groups like carboxyl, hydroxyl, amino and amide in many of common important molecules such as pharmaceuticals, biologically active substances, herbicides and environmental contaminants, this technique applies to a wide range of template molecules [28].

Up to now, many diverse techniques have been presented to synthesize MIPs [29–31]. Traditionally, MIPs were synthesized by a bulk polymerization technique. After polymerization, the resultant polymeric monoliths needed to be crushed, ground and sieved to generate particles in desired sizes [32,33]. This process is easy to perform, albeit time-consuming and laborious, which leads to low adsorption capacity and poor site accessibility to target molecules. These irregular particles generally exhibit less efficiency for various applications. Additionally, the imprinted sites may be destroyed during crushing and sieving processes [34]. In order to counterbalance such issues, several new synthetic techniques have been developed to produce monodispersed MIP particles [35,36]. Frequently, spherical polymeric particles are produced in high yields using these techniques, especially the precipitation polymerization method. Precipitation polymerization may be the simplest method, which is intriguing and straightforward for generation of microspherical and nanospherical MIPs because there is no need of any extra stabilizer, surfactant, emulsifier or suspending reagent.

Accordingly, the present work involves the precipitation polymerization as the synthesis method for dicamba-based MIPs to develop selective sorbents with improved morphology and recognition performance. To the best of authors' knowledge, the current research is the first attempt for the preparation of MIP nanoparticles using precipitation polymerization method particularly for the template dicamba to fabricate nanoscale-spherical imprinted polymers. The characteristics of the synthesized MIP were evaluated using differential scanning calorimetry, Fourier transform infrared (FTIR) spectroscopy, scanning electron microscopy (SEM) and Brunauer–Emmett–Teller (BET) methods. The effects of initial concentration, pH and adsorbent dosage on adsorption of dicamba from the water were investigated as well. The Langmuir, Freundlich, Sips, Temkin and Dubinin–Radushkevich models were employed to describe the equilibrium isotherms using non-linear regression analysis. Pseudo-first-order, Pseudo-second-order and Elovich kinetic models were also applied to describe the kinetic data.

2. Materials and methods

2.1. Materials

Dicamba (3,6-dichloro-2-methoxybenzoic acid), trimethylolpropane trimethacrylate (TRIM) and azobisisobutyronitrile (AIBN) were obtained from Sigma Aldrich (Steinheim, Germany). AIBN was re-crystallized from methanol before use. To remove the polymerization inhibitor, methacrylic acid (MAA; Darmstadt, Germany) was distilled in vacuum prior to being used. Acetonitrile (ACN), methanol and all the other solvents were HPLC grade, purchased from Merck and were used without further purification.

2.2. Synthesis of MIP nanoparticles

Molecularly imprinted nanoparticles were synthesized using precipitation polymerization. First, the template molecule, dicamba (DCA) (0.1 mmol), was dissolved in ACN (50 mL), in a thick-wall glass tube equipped with a screw cap followed by addition of the functional monomer, MAA (0.12 mmol). The mixture was homogeneously dispersed by sonication in an ultrasonic bath (VGT-1730 QTD, Korea) for 5 min. After that, the mixture was mixed gently for 15 min to create hydrogen-bonding interactions between MAA and DCA. After that, the cross-linker, TRIM (0.12 mmol), and the initiator, AIBN (0.0974 mmol), were added, and the solution was dispersed by sonication for another 5 min. The solution was then purged with N_2 gas for 15 min to get rid of oxygen in the solution, which could have retarded the synthesis process due to the annihilation of free radicals produced from the decomposition of the initiator. Subsequently, the reaction vessel was sealed under N_2 atmosphere. Finally, the polymerization process was carried out by inserting the reaction vessel in a water bath (Memmert, WB14, Germany). Also, for polymerization to take place, the temperature was increased from 25°C to 60°C within 1 h and after that kept for 23 h. After polymerization, polymer particles were collected by centrifugation (Hermle, Z36HK, Germany) at 21,000 rpm for 15 min. To remove the template from the polymer matrix, the unleached imprinted polymers were washed with a mixture of methanol/acetic acid (9:1, v/v) 5 times for 1 h until no template was detected in the washing solvent by

spectrometric measurement at 280 nm (Jenway, 6305, England). The template extraction of the polymer caused the cavities to be formed leading to the specific sorption of the template. In addition, the removal of other materials from the polymer took place (e.g., residual monomers or oligomers and initiator fragments). Residual acetic acid was removed with methanol. Moreover, the polymer particles were rinsed in the same volume of distilled water and acetone, and finally, the resulting leached imprinted polymers were dried in an oven at 50°C for 24 h. A schematic diagram of the molecular imprinting procedure is illustrated in Fig. 1. To verify that the adsorption of the template was due to molecular recognition instead of a non-specific binding, a control non-imprinted polymer (NIP) was also prepared according to the same procedure but without incorporating the target molecule, DCA.

2.3. Characterization of MIP nanoparticles

Thermal properties of polymer particles were investigated by a Mettler DSC 823 (Mettler Toledo, GmbH, Switzerland) equipped with a Julabo Thermocryostate Model FT100Y (Julabo Labortechnik, GmbH, Germany) under N_2 atmosphere. The samples were scanned at a heating rate of 10°C min^{-1} in a temperature range of 20°C–400°C. FTIR spectra (4,000–400 cm^{-1}) of DCA, unleached MIP, leached MIP and NIP were recorded on an FTIR spectrometer (Rayleigh, WQF-510A, China) using KBr pellets. The shape and the surface morphology of the polymers were estimated by SEM (TESCAN, VEGAII, Czech). To avoid any electric charging, polymeric particles were sputter coated with gold before the SEM measurement. The specific surface area, pore volume and average pore diameter of polymer particles were obtained by BET method (Bel, Belsorp-miniII, Japan). Before measurement, the samples were degassed at 100°C for 2 h before analysis under vacuum.

2.4. Adsorption experiments

To evaluate the adsorption affinity and recognition performance of the imprinted polymer in the aqueous solutions, the adsorption experiments were carried out in batch mode. For this purpose, the adsorption capacity (q_e) and the adsorption efficiency were employed to perform the primary calculations, which are given below:

$$q_e(\text{mg·g}^{-1}) = \frac{(C_i - C_e) \times V}{m} \tag{1}$$

$$\% \text{ Adsorption} = \frac{C_i - C_e}{C_i} \times 100 \tag{2}$$

where C_i and C_e (mg L^{-1}) are the initial and equilibrium concentrations of the DCA in the solution, respectively; V (mL) is the volume of the DCA solution; and m (mg) is the weight of the adsorbent. In order to compare the specific and non-specific interactions with DCA, a parallel procedure was performed using NIP particles. Note that all the experiments were performed in triplicate, and the reported data were the average of the obtained results.

2.4.1. Optimization of pH

The effect of pH on adsorption of DCA in water solutions was investigated to realize the optimum pH for the best adsorption performance. Therefore, the initial pH values of 300 mg L^{-1} of DCA in water solutions (at 25°C) were adjusted from 2 to 11 using HCl and NaOH. Then, 100 mg of the MIP and NIP were dispersed in 30 mL of each pH solution. The mixtures were shaken at 150 rpm for 3 h (Stuart, S1500, UK). The polymer particles were centrifuged at 21,000 rpm for 30 min, and then the supernatant was passed through an ultrafiltration membrane, and eventually, final concentrations
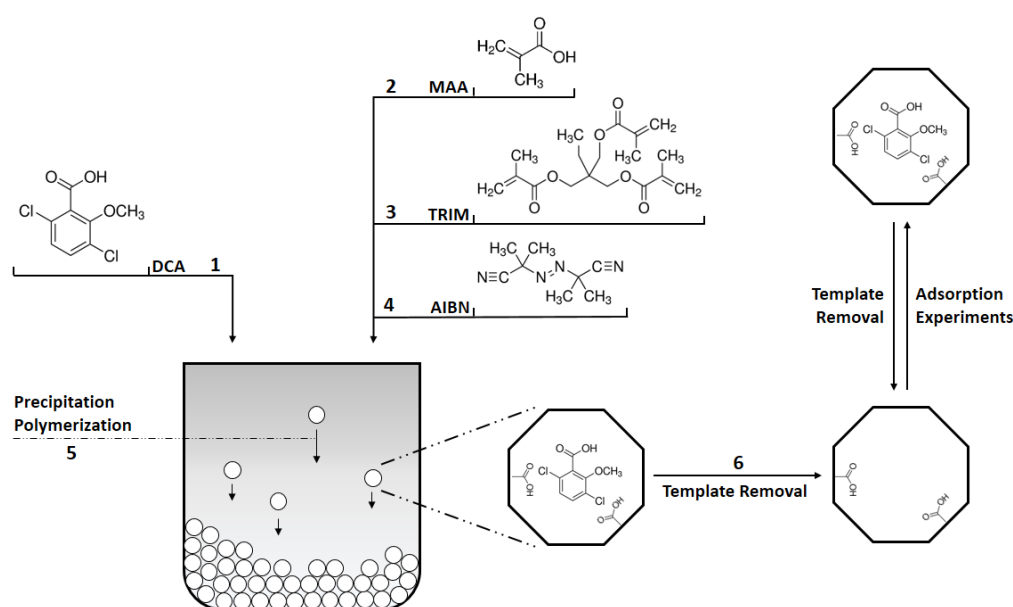

Fig. 1. Schematic diagram of the molecular imprinting procedure.

of DCA after the adsorption were determined by UV-visible spectrophotometer at 280 nm.

2.4.2. Optimization of adsorbent dosage

The dose of polymeric adsorbent was studied to determine the most effective amount of adsorbent on the adsorption of DCA in water solutions. Thus, different amounts of MIP nanoparticles (10, 25, 50, 100, 150 and 200 mg) were dispersed in 30 mL of 300 mg L^{-1} DCA in water solutions (at 25°C) at optimized pH, and the mixtures were shaken at 150 rpm for 3 h. After centrifugation and ultrafiltration, final concentrations of DCA in water solutions were determined by UV-visible spectrophotometer at 280 nm.

2.4.3. Study of adsorption kinetics

To appraise the effect of contact time on equilibrium adsorption of DCA in water solutions by the imprinted polymers, in dynamic adsorption conditions, the adsorption process was conducted through saturation studies at different times. In this case, the optimized dose of polymer particles was suspended in 30 mL of 300 mg L^{-1} DCA in water solution (at 25°C) at the optimized pH followed by shaking at 150 rpm for 30 min. The polymer particles were separated centrifugally, and after passing through an ultrafiltration membrane, the final concentration of DCA was analyzed by UV-visible spectrophotometer at 280 nm. The separated polymer particles were again suspended in 30 mL of the initial solution (300 mg L^{-1} DCA in water solution) according to the previous stage, and the final concentration of DCA was obtained in the next 30 min. This process was repeated 6 times per 30 min during 3 h. Afterward, the experimental data were analyzed to determine the adsorption kinetics using the pseudo-first-order, pseudo-second-order and Elovich kinetic models.

2.4.4. Study of adsorption isotherms

The equilibrium batchwise guest adsorption experiments were accomplished to evaluate the adsorption isotherms of polymer particles. Therefore, the optimized dose of polymer particles was mixed with 30 mL of DCA in water solutions (at 25°C) in different concentrations (300–2,000 mg L^{-1}) at the optimized pH followed by shaking at 150 rpm for the determined optimum time. The solutions were then analyzed to determine the final concentration of DCA after centrifugation and ultrafiltration using UV–visible spectrophotometer at 280 nm. Afterward, the experimental data were analyzed to determine the adsorption isotherms by using the Langmuir, Freundlich, Sips, Temkin and Dubinin-Radushkevich models.

2.4.5. Study of selectivity

To validate the selectivity of the synthesized MIP and NIP, 2,4-dichlorophenoxyacetic acid (2,4-D) and phenoxyacetic acid (POAC) were chosen as the competitors of DCA in competitive recognition studies (Fig. 2). The polymer (100 mg) was added to a flask containing 30 mL mixture of DCA, 2,4-D and POAC at a concentration of 300 mg L^{-1} (each of compounds) in aqueous solution (at 25°C), shaken

at room temperature for 3 h and then separated centrifugally. After filtration of the supernatant via an ultrafiltration membrane, the final concentration of DCA, 2,4-D and POAC in the supernatant was measured by UV-visible spectrophotometer at 280, 284 and 270 nm, respectively, for each compound.

3. Results and discussion

3.1. Characterization of MIP nanoparticles

3.1.1. Thermal analysis

Differential scanning calorimetry (DSC) analysis was performed to investigate the thermal characteristics of polymeric particles. Fig. 3 describes DSC plots of DCA, unleached and leached MIP and NIP. DSC thermograms of MIPs and NIP show that the decomposition process started approximately at 275°C. All polymers had similar thermal characteristics; however, an endothermic transition was observed at about 122°C for the unleached MIP (shown with arrow), which might be related to the melting process of the loaded DCA in unleached MIP.

3.1.2. Morphological analysis

The morphological structures of the MIP and NIP were detected by SEM. As can be seen in Fig. 4, spherical and nanoscale particles were obtained by the precipitation polymerization. The selection of polymerization technique is the main key point to synthesize MIP nanoparticles with a similar morphology. The average particle diameters of MIP and NIP nanoparticles are 234 nm (Fig. 4(a)) and 320 nm (Fig. 4(b)), respectively. The significant difference in the size of imprinted and NIPs could be attributed to the influence of template compound on the particle nucleation and growth
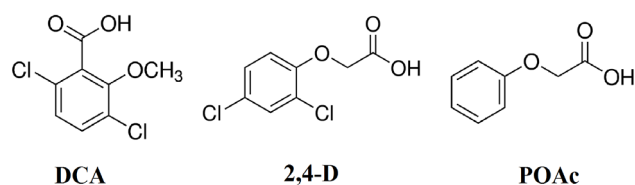

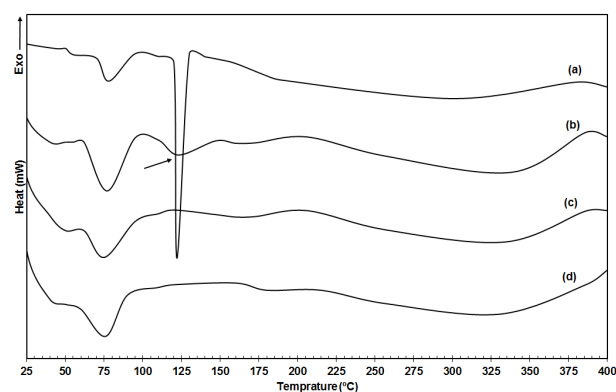Fig. 2. Chemical structure of template and template analog molecules.

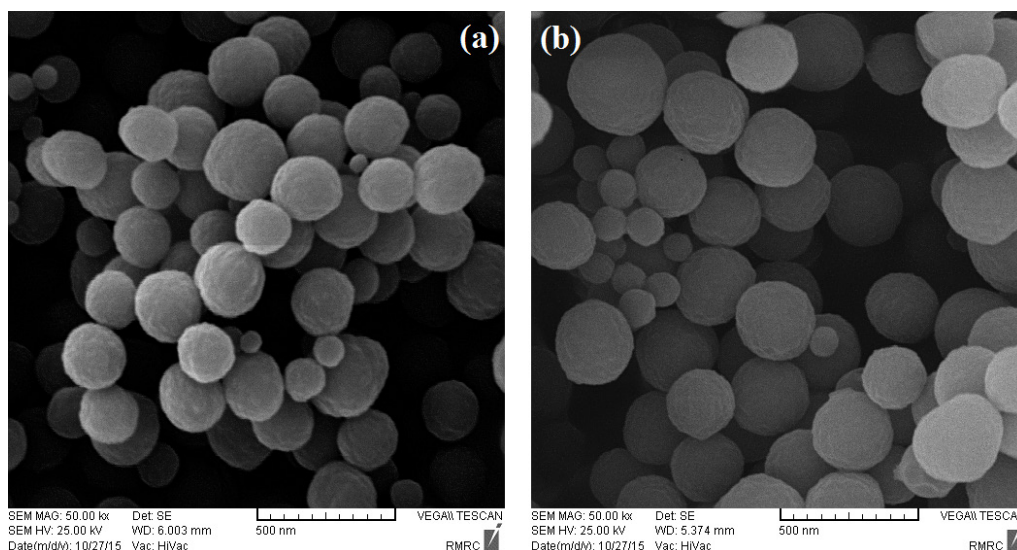Fig. 3. DSC thermograms of: (a) dicamba, (b) unleached MIP, (c) leached MIP and (d) NIP.

Fig. 4. Scanning electron micrographs of: (a) MIP and (b) NIP.

in the course of precipitation polymerization [36]. In the non-imprinting system, the functional monomer can form hydrogen-bonded dimers in the absence of DCA, and the pre-polymerization solution contains both functional monomer dimers and free functional monomer. In the imprinting system, there exist some molecular interactions between the functional monomer and DCA, which might somehow affect the growth of the cross-linked polymer nuclei resulting in smaller polymer beads [37]. Furthermore, the prepared nanoparticles are preferred over irregularly shaped particles in many applications particularly solid-phase microextraction, chemical sensors, capillary electrochromatography and biomedical applications [38].

3.1.3. BET analysis

Table 1 lists the specific surface areas, pore volumes and average pore diameters of MIP and NIP. The synthesized MIP and NIP had high specific surface areas resulting from their nanoporous structures. All the values of the specific surface area, pore size and volume of the MIP were higher than those of the NIP. In addition, the bigger pore diameter of MIP can provide DCA molecules more steric maneuverability within the pore. Thus, MIP nanospheres imprinted cavities are more easily accessible by DCA, which resulted in the higher adsorption capacity of the MIP than that of the NIP.

3.1.4. FTIR analysis

The MIP and NIP, obtained from polymerization process, were characterized using FTIR analyses to determine the functional groups present in the polymer matrices. The infrared spectra of unleached MIP, leached MIP and NIP are shown in Fig. 5. As can be seen, they displayed similar characteristic peaks indicating similarity in the backbone structure of different polymers. As a result of the hydrogen bonding with the –COOH group of MAA, the C=O stretching and the O–H stretching at 1,733 and 3,435 cm^{-1} in the leached MIP were shifted to 1,728 and 3,430 cm^{-1} in the

Table 1
Physical properties of MIP and NIP via BET analysis

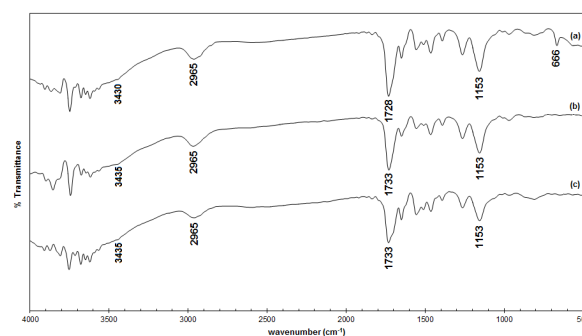| Physical properties	MIP	NIP
Specific surface area (m^2 g^{-1})	165.453	61.051
Pore volume (cm^3 g^{-1})	0.494	0.078
Average pore diameter (nm)	3.498	2.341

Fig. 5. FTIR spectra of: (a) unleached, (b) leached MIP and (c) NIP.

corresponding unleached MIP, respectively. Furthermore, in the unleached MIP, there was a sharp peak with low relative intensity at 666 cm^{-1}, which disappeared in the case of leached MIP and NIP. This peak is related to the stretching vibration of C–Cl bonds, indicating the fact that removal of the template from unleached MIP was very well done, and NIP was polymerized in the absence of template. The status of other peaks in each of the three types of polymers is similar: 1,153–1,263 cm^{-1} (symmetric and asymmetric stretching vibration of C–O bonds), 1,390 cm^{-1} (bending vibration of –CH$_3$ groups), 1,464 cm^{-1} (bending vibration of –CH$_2$ groups), 1,555 cm^{-1} (stretching vibration of C=C bonds) and 2,965 cm^{-1} (stretching vibration of C–H bonds).

3.2. Adsorption experiments

3.2.1. Optimization of pH

The effect of pH, as a substantial parameter in the imprinted and NIPs adsorption process, has to be studied because it influences both the properties of the MIP surface and the speciation of the target compound [39]. Hence, several batch experiments were performed by equilibrating 100 mg of the polymer nanoparticles with 30 mL of solutions containing 300 mg L^{-1} of DCA under the desired range of pH. Fig. 6 shows the effect of pH on the adsorption efficiency of DCA by MIP and NIP in the water medium. The adsorption efficiency of DCA by MIP and NIP remained approximately unchanged as the pH value of the solution varied from 2 to 7 whereas the adsorption efficiency was close to the maximum value in this pH range. This adsorption value suggests that the hydrophobic interactions and hydrogen bonding between DCA and the selective binding sites were the main driving forces for the adsorption. However, the adsorption efficiency of DCA by MIP and NIP was significantly decreased in the pH range of 9–11, in which the electrostatic repulsive interactions between DCA and the adsorbent overcome the binding affinity and hydrophobic interactions leading to a reduction in the value of adsorption [40,41]. It was also found that the MIP had higher sorption efficiency than the NIP over the entire pH range investigated, showing a good imprinting effect and adsorption performance. Therefore, further experiments were carried out using pH = 7 as the optimum.

3.2.2. Optimization of adsorbent dosage

Adsorbent dosage is a significant factor because it determines the capacity of an adsorbent to adsorb the adsorbate at a given initial concentration [42]. Therefore, the effect of adsorbent dosage was investigated by varying the amounts of polymer adsorbent from 10 to 200 mg in 30 mL of aqueous solutions containing 300 mg L^{-1} of DCA at the optimized pH. The results of dose optimization experiments are presented in Fig. 7. As can be seen, the adsorption efficiency of DCA by nanoparticles increases as the adsorbent dose is increased and became approximately constant after 100 mg of dose for both the MIP and NIP. From this point forth, the increment of adsorbent resulted in no considerable increase in the adsorption efficiency. Thus, the subsequent experiments were performed using 100 mg of adsorbent as the optimum dosage.

3.2.3. Study of adsorption kinetics

The adsorption capacities of MIP and NIP were evaluated at different times by taking samples every 30 min for 3 h followed by replacing the supernatant with fresh solution. As shown in Fig. 8, at the beginning, the adsorption occurred rapidly such that in the first 30 min, MIP and NIP bound 50.2% and 48% of their total adsorption, respectively. Then, it slowed down and reached 98.5% and 93.1% of their total adsorption, respectively, for MIP and NIP, in the following 90 min. For both MIP and NIP, the amount of adsorbed DCA was almost constant after 120 min, and equilibrium is reached. At the start of the adsorption process, the MIP beads had more adsorption sites for DCA, which allowed these imprinted cavities to catch the imprinted molecules, thereby

increasing the adsorption rate. However, as time proceeds, the number of adsorption sites decreased; the imprinted cavities of the surface were gradually saturated and occupied by DCA; and the adsorption rate was reduced, and also, the rate of
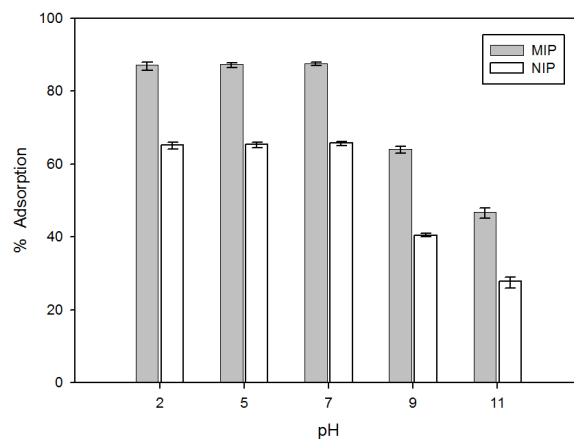
Fig. 6. Effect of pH on adsorption of dicamba by MIP and NIP in water solution (adsorbent dosage = 100 mg, C_i = 300 mg L^{-1}, T = 25°C).
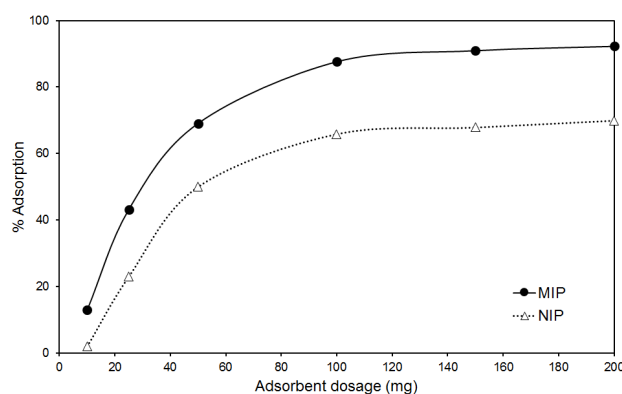
Fig. 7. Effect of adsorbent dosage on adsorption of dicamba by MIP and NIP in water solution (C_i = 300 mg L^{-1}, pH = 7, T = 25°C).
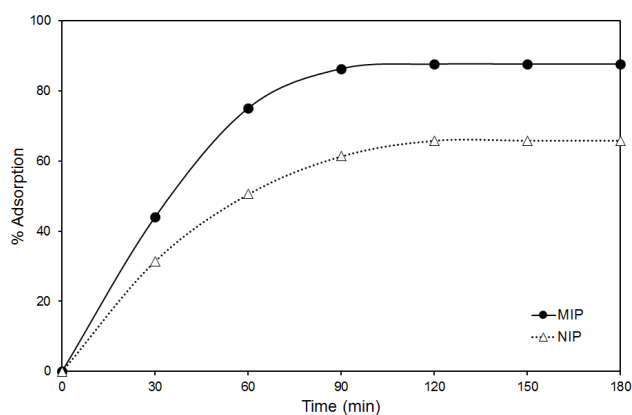
Fig. 8. Effect of contact time on adsorption of dicamba by MIP and NIP in water solution (adsorbent dosage = 100 mg, C_i = 300 mg L^{-1}, pH = 7, T = 25°C).

adsorption enhancement was decreased. Accordingly, the contact time of adsorption process was set to 120 min as the optimum. Furthermore, similar to static adsorption, in the case of dynamic adsorption experiments, the imprinted polymer had more adsorption capacity than NIP indicating that there were specific binding sites for DCA.

The kinetics of adsorption reveals more details about the performance and mechanisms of the adsorption process, and describes the rate of adsorbate uptake on adsorbent and controls the equilibrium time. Therefore, pseudo-first-order, pseudo-second-order and Elovich kinetic models were used to study the kinetics of adsorption process. The equations of the kinetic models are defined in Table 2. Experimental data and plots of the kinetic models are all presented in Fig. 9. All kinetic parameters of experimental data were calculated via non-linear regression and listed in Table 3. Using the non-linear regression method eliminates the problems with transformations of non-linear isotherm equations to linear forms (e.g., parameter estimation error and distortion of the fitting) [46]. It can be observed that the pseudo-first-order model fits better than the other models with the highest R^2, showing a good agreement between the calculated q_e and the experimental q_e values. Hence, the adsorption of DCA onto MIP and NIP may be physisorption. This may indicate that the adsorption of DCA takes place via surface exchange interactions until the surface functional sites are fully occupied [47]. Although the R^2 values of pseudo-second order and Elovich models are approximately acceptable, but the differences between the calculated q_e and the experimental q_e values are important to be worthy of attention. Therefore, it was found that the calculated q_e values are not in agreement with the experimental q_e values suggesting that the adsorption process does not follow the pseudo-second-order and Elovich models. As a conclusion, the adsorption kinetic data fitted the models in the order: pseudo-first order > pseudo-second order > Elovich.

3.2.4. Study of adsorption isotherms

The adsorption isotherms demonstrate the distribution of adsorbate molecules between the liquid phase and the solid phase, and the equilibrium relationships between adsorbate and adsorbent. Mathematical modeling can remarkably estimate the adsorption capacity and describe the adsorbent surface properties and affinity.

Therefore, five widely used models were employed to investigate which model can explicate the characteristics of the adsorption process better. Langmuir, Freundlich, Sips, Temkin and Dubinin–Radushkevich equations are defined in Table 4. The resulted fitting parameters have been obtained by using non-linear regression and given in Table 5. Fig. 10 represents the experimental data and the plots for the Langmuir, Freundlich, Sips, Temkin and Dubinin–Radushkevich isotherms fitting of the experimental data. From Fig. 10 and Table 5, it can be obviously seen that the experimental data of DCA adsorption onto MIP and NIP fitted well with the Sips equation, which was statistically confirmed by the greater R^2 values more proximate to unity. Also, the calculated values of R^2 in Freundlich model were not satisfactory indicating a poor fit. While Langmuir model assumes a monolayer adsorption that the adsorbent adsorbs the adsorbates on identical and energetically equivalent sites on the homogeneous surface, Freundlich model supposes a non-ideal and reversible adsorption, not only limited to monolayer but also multilayer adsorption with non-uniform distribution of adsorption sites and affinities on the heterogeneous surface [57]. Sips model is a hybrid model of Freundlich and Langmuir models for analyzing the heterogeneous adsorption systems that at low
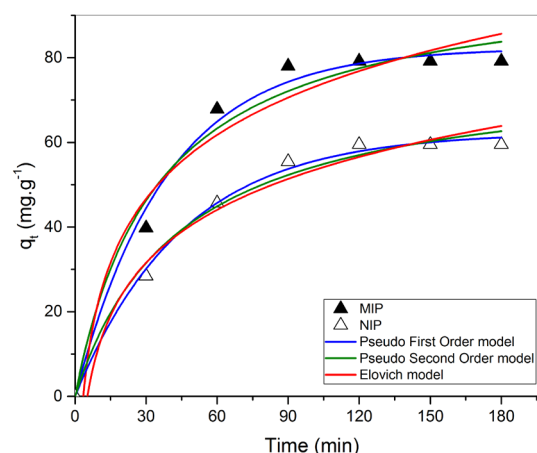

Fig. 9. Kinetic models curves for adsorption of dicamba by MIP and NIP in water solution (adsorbent dosage = 100 mg, C_i = 300 mg L^{-1}, pH = 7, T = 25°C).

Table 2
Equations and parameters of kinetic models

Kinetic models	Equation	Parameters	Ref.
Pseudo-first order	$q_t = q_e(1 - e^{-k_1 t})$	q_t (mg g^{-1}): the amount of adsorbate adsorbed at time t q_e (mg g^{-1}): the amount of solute sorbed at equilibrium k_1 (min^{-1}): the rate constant of first-order sorption	[43]
Pseudo-second order	$q_t = \dfrac{k_2 q_e^2 t}{1 + k_2 q_e t}$	k_2 (g mg^{-1} min^{-1}): the rate constant of second-order sorption	[44]
Elovich	$q_t = \dfrac{1}{\beta_E}\ln(\alpha_E \beta_E) + \dfrac{1}{\beta_E}\ln t$	α_E (mg g^{-1} min^{-1}): initial sorption rate β_E (g mg^{-1}): related to the extended of surface coverage and activation energy for chemisorption	[45]

and high adsorbate concentrations show the characteristics of the Freundlich and Langmuir models, respectively [58]. From the Langmuir model with acceptable R^2, the essential

Table 3
Kinetic parameters for DCA adsorption onto MIP and NIP (C_i = 300 mg L^{-1}; pH = 7; T = 25°C)

Kinetic models	Parameters	MIP	NIP
Pseudo-first-order model	$q_{e,exp}$ (mg g^{-1})	79.1739	59.4783
	$q_{e,cal}$ (mg g^{-1})	82.2759	62.3192
	k_1 (min^{-1})	0.02591	0.0220
	R^2	0.989	0.996
Pseudo-second-order model	$q_{e,cal}$ (mg g^{-1})	99.9572	78.0757
	k_2 (g mg^{-1} min^{-1})	0.0287	0.0225
	R^2	0.973	0.986
Elovich model	α_E (mg g^{-1} min^{-1})	6.1930	3.4551
	β_E (g mg^{-1})	0.0459	0.0554
	R^2	0.958	0.977

parameter of the Langmuir model, R_L, is in the range of 0–1, indicating that the sorption of DCA on MIP and NIP is favorable. From Sips model, q_m describes the total number of binding sites (N_t) and has a higher value for MIP than NIP, which reveals that MIP had a higher concentration of binding sites per gram. This may be explained by the presence of the template in polymerization, which leads to the specificity for DCA. Moreover, MIP was more homogeneous (m = 0.7974) as compared with NIP (m = 0.7245), which is due to the imprinting. Temkin model suggests that because of adsorbent–adsorbate interactions, the heat of adsorption is decreased for all molecules in the layer with coverage, and the adsorption is described by a uniform distribution of binding energies, up to some maximum binding energy [59]. However, Temkin model did not give a good fit for both MIP and NIP with low R^2 values. Dubinin–Radushkevich model explains the adsorption process with a Gaussian energy distribution onto a heterogeneous surface and investigates the type of adsorption mechanism with its mean free energy of adsorption, E, which is defined as the free energy for the transfer of per mole of the adsorbate from the infinity in the solution

Table 4
Equations and parameters of adsorption isotherms

Adsorption isotherm	Equation	Parameters	Ref.
Langmuir	$q_e = \dfrac{q_m K_L C_e}{1 + K_L C_e}$	q_e (mg·g^{-1}): equilibrium adsorption capacity	[47,48]
		q_m (mg g^{-1}): maximum adsorption capacity of the adsorbent	
		K_L (L g^{-1}): Langmuir constant related to adsorption affinity	
		C_e (mg L^{-1}): equilibrium concentration of the solute	
	$R_L = \dfrac{1}{1 + K_L C_i}$	R_L: separation factor	
		$R_L > 1$: unfavorable isotherm	
		$R_L = 1$: linear isotherm	
		$0 < R_L < 1$: favorable isotherm	
		$R_L = 0$: irreversible isotherm	
		C_i (mg L^{-1}): initial concentration of the solute	
Freundlich	$q_e = K_F C_e^{\,m}$	K_F (mg g^{-1})(mg L^{-1})$^{-m}$: Freundlich constant related to adsorption capacity	[49,50]
		m: surface heterogeneity	
		$0 \le m \le 1$: closer to 1 as Heterogeneity decreases	
		$m = 1$: homogeneous system	
		$m < 1$: physisorption	
		$m > 1$: chemisorption	
Sips	$q_e = \dfrac{q_m K_s C_e^{\,m}}{1 + K_s C_e^{\,m}}$	K_s (L g^{-1}): Sips constant related to adsorption affinity	[51,52]
Temkin	$q_e = \dfrac{RT}{\beta_T}\ln(\alpha_T C_e)$	α_T: Temkin constant related to the maximum binding energy	[53]
		β_T: Temkin constant related to the heat of adsorption	
Dubinin-Radushkevich	$q_e = q_m e^{(-K_{DR}\varepsilon^2)}$	K_{DR} (mol^2 kJ^{-2}): Dubinin–Radushkevich constant related to free energy	[54,55]
	$\varepsilon = RT\ln\left(1 + \dfrac{1}{C_e}\right)$	R (J mol^{-1} K^{-1}): universal gas constant, 8.314	
		T (K): absolute solution temperature	
		ε: Polanyi potential	
	$E = \dfrac{1}{\sqrt{2K_{DR}}}$	E (kJ mol^{-1}): mean free energy of adsorption	

Table 5
Isotherm models parameters for DCA adsorption onto MIP and NIP (C_i = 300 – 2,000 mg L^{-1}; pH = 7; T = 25°C)

| Isotherm models	Parameters	MIP	NIP
Langmuir	q_m (mg g^{-1})	275.4897	143.2306
	K_L (L g^{-1})	0.0126	0.0079
	R_L	0.038–0.209	0.059–0.297
	R^2	0.987	0.945
Freundlich	K_F (mg g^{-1}) (mg L^{-1})$^{-m}$	44.7141	26.4442
	m	0.2554	0.2244
	R^2	0.809	0.749
Sips	q_m (mg g^{-1})	259.0993	132.6010
	K_s (L g^{-1})	0.0048	0.00135
	m	0.7974	0.7245
	R^2	0.997	0.958
Temkin	α_T	0.1791	0.1508
	β_T	51.0635	25.3259
	R^2	0.910	0.835
Dubinin–Radushkevich	q_m (mg g^{-1})	219.6008	119.8113
	K_{DR} (mol^2 kJ^2)	0.0181	0.0379
	E (kJ mol^{-1})	5.2559	3.6322
	R^2	0.847	0.875
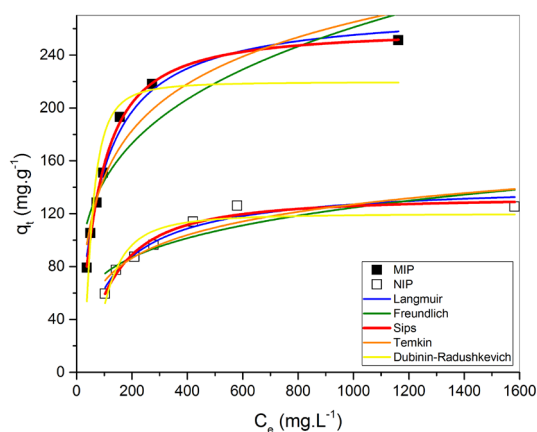
Fig. 10. Adsorption isotherms curves for adsorption of dicamba by MIP and NIP in water solution (adsorbent dosage = 100 mg, C_i = 300 mg L^{-1}, pH = 7, T = 25°C).

to the surface of the adsorbent [56]. When the value of E is less than 8 kJ mol^{-1}, it represents physisorption [60]; the value of E in the range of 8–16 kJ mol^{-1} implies that the adsorption mechanism follows ion exchange [61], and the value higher than 20 kJ mol^{-1} represents the chemisorption [62]. The calculated values of E for the DCA adsorption for both MIP and NIP are below 8 kJ mol^{-1} indicating that the adsorption mechanism of DCA onto the nanoparticles' surfaces follow the physical adsorption type. As a conclusion, the adsorption isotherm data fitted the models in the order: Sips > Langmuir > Temkin > Dubinin–Radushkevich > Freundlich.

3.2.5. Study of selectivity

In order to evaluate the selectivity of the synthesized MIP and NIP, 2,4-D and POAC were selected as the potential competitors, as template analogs, because of the similarity of their chemical structures to DCA. DCA is commonly used along with 2,4-D. 2,4-D is a common systemic herbicide used in the control of broadleaf weeds. It is also one of the most widely used herbicides worldwide [63]. POAC is the main skeleton of plant growth regulators and herbicides, which is used as an intermediate for manufacturing pesticides and fungicides and also has other applications [64]. The results of the adsorption experiments are shown in Fig. 11. In order to study the molecular recognition ability of the imprinted polymers toward template analogs, the selectivity factor (α) was evaluated using the following equation:

$$\alpha = \frac{q_{\text{DCA}}}{q_{\text{analog}}} \tag{3}$$

where q_{DCA} represents the adsorption capacity of DCA, and q_{analog} stands for the adsorption capacity of the analogs, 2,4-D and POAC. The results are provided in Table 6. As shown in Fig. 11, the adsorption capacity of DCA on MIP is much higher than that of 2,4-D and POAC, and that of NIP. The results propose the presence of specific imprinted sites for adsorption of the target molecule. MIPs have memory cavities with fixed size, shape and binding sites that can recognize their target molecules through them. The shape of the binding cavity and the strength of the specific binding interactions between the target molecules and the binding sites determine the selectivity of MIPs [65,66]. As a result, the decreased adsorption capacities could be due to the
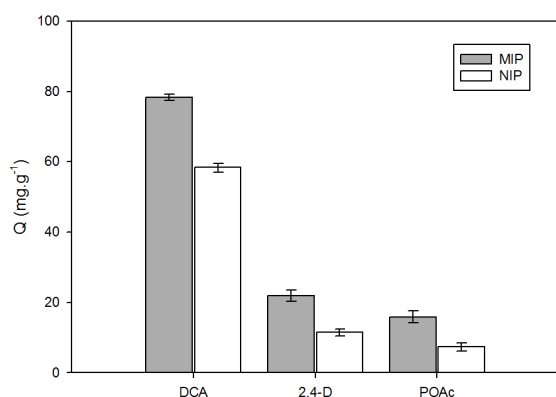
Fig. 11. Competitive adsorption of MIP and NIP for template and template analog (adsorbent dosage = 100 mg, C_i = 300 mg L^{-1}, pH = 7, T = 25°C).

Table 6
Selectivity factor of the MIP and NIP toward template analogs (C_i = 300 mg L^{-1}; pH = 7; T = 25°C)

Template analog	Selectivity factor (α)	
	MIP	NIP
2,4-D	3.4	4.6
POAC	4.5	6.7

mismatch of the structure and size of the template analog molecules with the MIP cavities and unspecific interactions. It demonstrates that DCA is responsible for the creation of binding pockets of definite shape and selectivity, and better adsorption performance in the MIP.

4. Conclusions

In this study, novel spherical dicamba imprinted polymer nanoparticles were successfully synthesized for the first time via the precipitation polymerization method using MAA as the functional monomer, TRIM as the cross-linker, ACN as the polymerization solvent and AIBN as the initiator. The imprinted polymer showed attractive characteristics including spherical morphology, high adsorption capacity and selectivity. Thus, the MIP can be effectively used for recognition, determination and adsorption of dicamba from the water. It was also confirmed that the porosity of MIPs plays an important role in their adsorption properties. Moreover, Sips isotherm fitted well with the equilibrium adsorption data. In addition, the pseudo-first-order kinetic model agrees very well with the dynamic experimental data for dicamba adsorption demonstrating the physical adsorption process of dicamba from aqueous solutions.

References

[1] J. Popp, K. Peto, J. Nagy, Pesticide productivity and food security. A review, Agron. Sustain. Dev., 33 (2013) 243–255.
[2] E.H. Shin, J.H. Choi, A.M. Abd El-Aty, S. Khay, S.J. Kim, M.H. Im, C.H. Kwon, J.H. Shim, Simultaneous determination of three acidic herbicide residues in food crops using HPLC and confirmation via LC-MS/MS, Biomed. Chromatogr., 25 (2011) 124–135.
[3] Y. Yamada, Report of the Joint Meeting of the FAO Panel of Experts on Pesticide Residues in Food and the Environment and the WHO Core Assessment Group on Pesticide Residues, FAO Plant Production and Protection Paper, Rome, Italy, September 21–30, 2010, FAO, Rome.
[4] S.D. Comfort, W.P. Inskeep, R.E. Macur, Retention of dissolved organic carbon and sulfate in aggregated acid forest soils, J. Environ. Qual., 21 (1992) 653–658.
[5] D.J. Hamilton, Á. Ambrus, R.M. Dieterle, A.S. Felsot, C.A. Harris, P.T. Holland, A. Katayama, N. Kurihara, J. Linders, J. Unsworth, S.S. Wong, Regulatory limits for pesticide residues in water (IUPAC Technical Report), Pure Appl. Chem., 75 (2003) 1123–1155.
[6] C. Alexander, H.S. Andersson, L.I. Andersson, R.J. Ansell, N. Kirsch, I.A. Nicholls, J. O'Mahony, M.J. Whitcombe, Molecular imprinting science and technology: a survey of the literature for the years up to and including 2003, J. Mol. Recognit., 19 (2006) 106–180.
[7] L. Chen, S. Xua, J. Li, Recent advances in molecular imprinting technology: current status, challenges and highlighted applications, Chem. Soc. Rev., 40 (2011) 2922–2942.
[8] E.L. Holthoff, F.V. Bright, Molecularly templated materials in chemical sensing, Anal. Chim. Acta, 594 (2007) 147–161.
[9] H.H. Yang, S.Q. Zhang, F. Tan, Z.X. Zhuang, X.R. Wang, Surface molecularly imprinted nanowires for biorecognition, J. Am. Chem. Soc., 127 (2005) 1378–1379.
[10] C. He, F. Liu, K. Li, H. Liu, Molecularly imprinted polymer film grafted from porous silica for selective recognition of testosterone, Anal. Lett., 39 (2006) 275–286.
[11] Q. Fu, N. Zheng, Y.Z. Li, W.B. Chang, Z.M. Wang, Molecularly imprinted polymers from nicotinamide and its positional isomers, J. Mol. Recognit., 14 (2001) 151–156.
[12] X.D. Huang, H.F. Zou, X.M. Chen, Molecularly imprinted monolithic stationary phases for liquid chromatographic separation of enantiomers and diastereomers, J. Chromatogr. A, 984 (2003) 273–282.
[13] B.W. Sun, Y.Z. Li, W.B. Chang, Molecularly imprinted polymer using p-hydroxybenzoic acid, p-hydroxyphenylacetic acid and p-hydroxyphenylpropionic acid as templates, J. Mol. Recognit., 14 (2001) 388–392.
[14] I. Chianella, S.A. Pilesky, I.E. Tothill, B. Chen, A.P.F. Turner, MIP-based solid phase extraction cartridges combined with MIP-based sensors for the detection of microcystin-LR, Biosens. Bioelectron., 18 (2003) 119–127.
[15] G. Theodoridis, A. Kantifes, P. Manesiotis, N. Raikos, H.T. Papadopoulou, Preparation of a molecularly imprinted polymer for the solid-phase extraction of scopolamine with hyoscyamine as a dummy template molecule, J. Chromatogr. A, 987 (2003) 103–109.
[16] F. Puoci, M. Curcio, G. Cirillo, F. Lemma, U.G. Spizzirri, N. Picci, Molecularly imprinted solid-phase extraction for cholesterol determination in cheese products, Food Chem., 106 (2008) 836–842.
[17] K.C. Ho, W.M. Yeh, T.S. Tung, J.Y. Liao, Amperometric detection of morphine based on poly(3,4-ethylenedioxythiophene) immobilized molecularly imprinted polymer particles prepared by precipitation polymerization, Anal. Chim. Acta, 542 (2005) 90–96.
[18] M. Javanbakht, S. Eynollahi Fard, A. Mohammadi, M. Abdouss, M.R. Ganjali, P. Norouzi, L. Safaraliee, Molecularly imprinted polymer based potentiometric sensor for the determination of hydroxyzine in tablets and biological fluids, Anal. Chim. Acta, 612 (2008) 65–74.
[19] A. Cui, A. Singh, D.L. Kaplan, Enzyme-based molecular imprinting with metals, Biomacromolecules, 3 (2002) 1353–1358.

[20] R.N. Karmalkar, M.G. Kulkarni, R.A. Mashelkar, Pendent chain linked delivery systems: II. Facile hydrolysis through molecular imprinting effects, J. Controlled Release, 43 (1997) 235–243.

[21] W. Chen, D.K. Han, K.D. Ahn, J.M. Kim, Molecularly imprinted polymers having amidine and imidazole functional groups as an enzyme-mimetic catalyst for ester hydrolysis, Macromol. Res., 10 (2002) 122–126.

[22] S. Ashrafian, S.A. Ataei, M. Jahanshahi, Novel composite membranes embedded with molecularly imprinted porous polymeric nanospheres for targeted phenol, Polym. Adv. Technol., 27 (2016) 789–804.

[23] R. Suedee, T. Srichana, G.J. Martin, Evaluation of matrices containing molecularly imprinted polymers in the enantioselective-controlled delivery of β-blockers, J. Controlled Release, 66 (2000) 135–147.

[24] H. Sambe, K. Hoshina, R. Moadel, W. Wainer, J. Haginaka, Simultaneous determination of bisphenol A and its halogenated derivatives in river water by combination of isotope imprinting and liquid chromatography–mass spectrometry, J. Chromatogr. A, 1134 (2006) 16–23.

[25] C.J. Allender, C. Richardson, B. Woodhouse, C.M. Heard, K.R. Brain, Pharmaceutical applications for molecularly imprinted polymers, Int. J. Pharm., 195 (2000) 39–43.

[26] M. Masoumi, M. Jahanshahi, Synthesis and recognition of nano pore molecularly imprinted polymers of thymol on the surface of modified silica nanoparticles, Adv. Polym. Technol., 35 (2016) 221–227.

[27] O. Brüggemann, Molecularly imprinted materials – receptors more durable than nature can provide, Adv. Biochem. Eng./ Biotechnol., 76 (2002) 127–163.

[28] O. Kotrotsiou, S. Chaitidou, C. Kiparissides, Boc-l-tryptophan imprinted polymeric microparticles for bioanalytical applications, Mater. Sci. Eng., C, 29 (2009) 2141–2146.

[29] R.C. Martinez, E.R. Gonzalo, E.H. Hernández, M.E.D. García, Development and characterisation of a molecularly imprinted polymer prepared by precipitation polymerization for the determination of phenylurea herbicides, J. Sep. Sci., 28 (2005) 453–461.

[30] N. Pérez, M.J. Whitcombe, E.N. Vulfson, Molecularly imprinted nanoparticles prepared by core-shell emulsion polymerization, J. Appl. Polym. Sci., 77 (2000) 1851–1859.

[31] M. Lehmann, H. Brunner, G.E.M. Tovar, Selective separations and hydrodynamic studies: a new approach using molecularly imprinted nanosphere composite membranes, Desalination, 149 (2002) 315–321.

[32] G. Wulff, A. Biffis, Molecular Imprinting with Covalent or Stoichiometric Non-Covalent Interactions, B. Sellergren, Ed., Molecularly Imprinted Polymers: Man-made Mimics of Antibodies and their Applications in Analytical Chemistry, Elsevier, Amsterdam, 2001, pp. 79–80.

[33] Y. Liu, K. Hoshina, J. Haginaka, Monodispersed, molecularly imprinted polymers for cinchonidine by precipitation polymerization, Talanta, 80 (2010) 1713–1718.

[34] C.M. Dai, X.F. Zhou, Y.L. Zhang, S.G. Liu, J. Zhang, Synthesis by precipitation polymerization of molecularly imprinted polymer for the selective extraction of diclofenac from water samples, J. Hazard. Mater., 198 (2011) 175–181.

[35] A. Poma, A.P. Turner, S.A. Piletsky, Advances in the manufacture of MIP nanoparticles, Trends Biotechnol., 28 (2010) 629–637.

[36] K. Yoshimatsu, K. Reimhult, A. Krozer, K. Mosbach, K. Sode, L. Ye, Uniform molecularly imprinted microspheres and nanoparticles prepared by precipitation polymerization: the control of particle size suitable for different analytical applications, Anal. Chim. Acta, 584 (2007) 112–121.

[37] M. Esfandyari-Manesh, M. Javanbakht, F. Atyabi, R. Dinarvand, Synthesis and evaluation of uniformly sized carbamazepine-imprinted microspheres and nanospheres prepared with different mole ratios of methacrylic acid to methyl methacrylate for analytical and biomedical applications, J. Appl. Polym. Sci., 125 (2012) 1804–1813.

[38] M. Esfandyari-Manesh, M. Javanbakht, F. Atyabi, A. Mohammadi, S. Mohammadi, B. Akbari-Adergani, R.

[39] Q. Yu, S. Deng, G. Yu, Selective removal of perfluorooctane sulfonate from aqueous solution using chitosan-based molecularly imprinted polymer adsorbents, Water Res., 42 (2008) 3089–3097.

[40] C. Dai, S.U. Geissen, Y.L. Zhang, Y.J. Zhang, X.F. Zhou, Selective removal of diclofenac from contaminated water using molecularly imprinted polymer microspheres, Environ. Pollut., 159 (2011) 1660–1666.

[41] S.C. Lee, F.L. Chuang, Y.L. Tsai, H. Chen, Studies on the preparation and properties of sol-gel molecularly imprinted polymer based on tetraethoxysilane for recognizing sulfonamides, J. Polym. Res., 17 (2010) 737–744.

[42] E. Demirbas, N. Dizge, M.T. Sulak, M. Kobya, Adsorption kinetics and equilibrium of copper from aqueous solutions using hazelnut shell activated carbon, Chem. Eng. J., 148 (2009) 480–487.

[43] S. Langergen, B.K. Svenska, About the theory of so-called adsorption of soluble substances, Handlingar, 24 (1898) 1–39.

[44] Y.S. Ho, G. Mckay, Pseudo-second order model for sorption processes, Process Biochem., 34 (1999) 451–465.

[45] M.M. Castro Lopez, M.C. Cela Perez, M.S. Dopico Garcia, J.S. Lopez Vilarino, M.V. Gonzalez Rodriguez, L.F. Barral Losada, Preparation, evaluation and characterization of quercetin-molecularly imprinted polymer for preconcentration and clean-up of catechins, Anal. Chim. Acta, 721 (2012) 68–78.

[46] J. Srenscek-Nazzal, U. Narkiewicz, A.W. Morawski, R.J. Wrobel, B. Michalkiewicz, Comparison of optimized isotherm models and error functions for carbon dioxide adsorption on activated carbon, J. Chem. Eng. Data, 60 (2015) 3148–3158.

[47] E. Bulut, M. Ozacar, I. Ayhan Sengil, Equilibrium and kinetic data and process design for adsorption of Congo Red onto bentonite, J. Hazard. Mater., 154 (2008) 613–622.

[48] I. Langmuir, The constitution and fundamental properties of solids and liquids, J. Am. Chem. Soc., 38 (1916) 2221–2295.

[49] T.W. Webber, R.K. Chakkravorti, Pore and solid diffusion models for fixed-bed adsorbers, AIChE J., 20 (1974) 787–794.

[50] H.M.F. Freundlich, Over the adsorption in solution, J. Phys. Chem., 57 (1906) 385–471.

[51] A.A. Atia, A.M. Donia, A.M. Yousif, Removal of some hazardous heavy metals from aqueous solution using magnetic chelating resin with iminodiacetate functionality, Sep. Purif. Technol., 61 (2008) 348–357.

[52] R. Sips, On the structure of a catalyst surface, J. Phys. Chem., 16 (1948) 490–495.

[53] J.R. Memon, S.Q. Memon, M.I. Bhanger, M.Y. Khuhawar, G.C. Allen, G.Z. Memon, A.G. Pathan, Efficiency of Cd(II) removal from aqueous media using chemically modified polystyrene foam, Eur. Polym. J., 44 (2008) 1501–1511.

[54] M.I. Temkin, V. Pyzhev, Kinetics of ammonia synthesis on promoted iron catalyst, Acta Phys. Chim. USSR, 12 (1940) 327–356.

[55] M.M. Dubinin, L.V. Radushkevich, The equation of the characteristic curve of the activated charcoal, Proc. Acad. Sci. USSR Phys. Chem. Sect., 55 (1947) 331–337.

[56] J.P. Hobson, Physical adsorption isotherms extending from ultra high vacuum to vapor pressure, J. Phys. Chem., 73 (1969) 2720–2727.

[57] K.Y. Foo, B.H. Hameed, Insights into the modeling of adsorption isotherm systems, Chem. Eng. J., 156 (2010) 2–10.

[58] A.B. Pérez-Marín, V. Meseguer Zapata, J.F. Ortuno, M. Aguilar, J. Sáez, M. Llorens, Removal of cadmium from aqueous solutions by adsorption onto orange waste, J. Hazard. Mater., 139 (2007) 122–131.

[59] C. Aharoni, M. Ungarish, Kinetics of activated chemisorption. Part 2. Theoretical models, J. Chem. Soc., Faraday Trans., 73 (1977) 456–464.

[60] S. Kundu, A.K. Gupta, Arsenic adsorption onto iron oxide-coated cement (IOCC): regression analysis of equilibrium data with several isotherm models and their optimization, Chem. Eng. J., 122 (2006) 93–106.

[61] F. Helfferich, Ion Exchange, McGraw-Hill Book Company, New York, 1962.

[62] H. Chen, G. Dai, J. Zhao, A. Zhong, J. Wu, H. Yan, Removal of copper(II) ions by a biosorbent – *Cinnamomum camphora* leaves powder, J. Hazard. Mater., 177 (2010) 228–236.

[63] D. Loomis, K. Guyton, Y. Grosse, F. El-Ghissasi, V. Bouvard, L. Benbrahim-Tallaa, N. Guha, H. Mattock, K. Straif, Carcinogenicity of lindane, DDT, and 2,4-dichlorophenoxyacetic acid, Lancet Oncol., 16 (2015) 891–892.

[64] T. Cserháti, E. Forgács, Phenoxyacetic acids: separation and quantitative determination, J. Chromatogr. B, 717 (1998) 157–178.

[65] N.W. Turner, E.V. Piletska, K. Karim, M. Whitcombe, M. Malecha, N. Magan, C. Baggiani, S.A. Piletsky, Effect of the solvent on recognition properties of molecularly imprinted polymer specific for ochratoxin A, Biosens. Bioelectron., 20 (2004) 1060–1067.

[66] Y. Liu, F. Wang, T. Tan, M. Lei, Study of the properties of molecularly imprinted polymers by computational and conformational analysis, Anal. Chim. Acta, 581 (2007) 137–146.